2011 IEEE International Conference on Robotics and Automation
Shanghai International Conference Center
May 9-13, 2011, Shanghai, China

A Cable Driven Upper Arm Exoskeleton for Upper Extremity Rehabilitation

Ying Mao and Sunil K. Agrawal
Department of Mechanical Engineering
University of Delaware
Newark, DE 19716, USA, Contact: agrawal@udel.edu

***Abstract*— Conventional robotic rehabilitation devices for upper extremity are bulky, heavy or lack the ability to provide joint level rehabilitation. Some designs address these issues by replacing rigid links of the exoskeletons with light weight cables. However these designs are controlled in position mode instead of force control which is desirable for rehabilitation. In this paper, a 5 degree-of-freedom cable-driven upper arm exoskeleton, with control of force, is proposed. In this design, attachment points of cables on the arm are adjustable. The attachment points are optimized to achieve large workspace to perform activities of daily living. Simulation results of force field control for training and rehabilitation of the arm are presented. Experiments have been performed on a dummy robotic arm in the upper arm exoskeleton.**

I. Introduction

Studies have shown that highly repetitive task-oriented movement training [1] positively affects the recovery of neuromuscular functions of the arm and in the activities of daily living(ADLs) [2]. Robotic rehabilitation has become increasingly popular due to its cost effectiveness and capability of controlled training.

Current robotic rehabilitation devices for the upper extremity can be classified into end-effector interacting devices and exoskeletal devices. Devices of the first category include MIT-Manus [3] and MIME [4]. These add small mass and inertia to the patient's limb during motion. However, these devices lack joint level rehabilitation capability as the interaction with human is at the end-effector. On the other hand, the exoskeletal devices, such as Armin [5], MGA [6] and MAHI [7], have rigid links attached to the human arm and motors at exoskeletal joints. This makes joint level control possible, however, introduces large mass to the human arm. This changes the dynamics of human arm which results in changes in motion. Some designs, such as [8-9], have attempted to reduce the mass and inertia by placing the motors away from the joints using cables and pulleys to actuate the joints. However, rigid links are used in these designs but these only partially reduce the mass. Also, the requirement for the exoskeletons to precisely align the joints with human joints brings in additional complexity.

Yang et al. designed a 7 degree-of-freedom (DOF) cable-driven exoskeleton wearable by the human arm [10]. Instead of using rigid links, this design adopted several light-weight cuffs attached to the human arm. Cables attached to these cuffs are used to actuate the exoskeleton. Such a design provides control of the full arm, has low mass, and does not require careful joint alignment due to the absence of rigid links. A 4-DOF cable-driven upper arm exoskeleton was developed at University of Delaware [13-14]. The goal of the design was to control the tensions with the cable system, which is necessary for rehabilitation [13]. However, the design was limited to position control due to the motor amplifier.

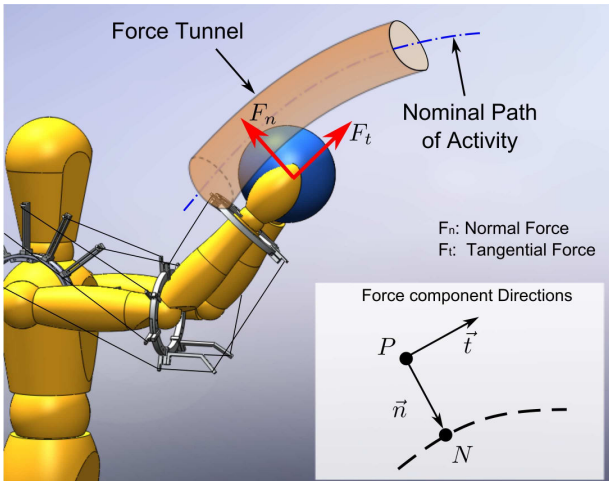

Fig. 1. A user performs training task with the exoskeleton. Force field is provided to assist the user.

This paper presents a 5-DOF cable-driven upper arm exoskeleton, developed in the Mechanical System Laboratory at University of Delaware. This design differs from existing designs in that it aims to achieve force control. The motors run in torque mode and a load cell is connected in series with each cable to measure and control the cable tension. Force field control, which has been shown successful [14], was implemented on the exoskeleton. Fig. 1 shows a sketch of a user performing a training task with the exoskeleton. A force field is provided to assist the user performing ADLs. Detailed exoskeleton design, electronics, workspace optimization, the force field control architecture and simulation results are presented. Experiments were carried with five healthy subjects. Results show that the force field controller is able to keep the subjects closer to the nominal path.

II. System Design and Model

A. Exoskeleton Design

The sketch of the cable-driven upper arm exoskeleton and the coordinate frames are shown in Fig. 2. The exoskeleton

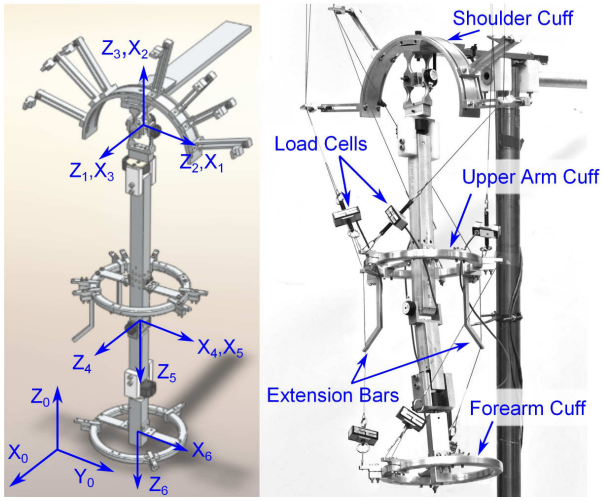

Fig. 2. Left: CAD model of the upper arm exoskeleton and coordinate frames. Right: Photograph of the exoskeleton prototype.

has the ability to control 5 degrees-of-freedom, three at the shoulder, one DOF elbow flexion and extension, and one DOF forearm pronation and supination. The DH Parameters of the exoskeleton are shown in Table I. Please note that link 1 has a fictitious joint which rotates the base frame to align it in a convenient direction.

TABLE I

DH PARAMETERS FOR ARM EXOSKELETON

Link	a_i	α_i	d_i	q_i
1	0	$\frac{\pi}{2}$	0	$\frac{\pi}{2}$
2	0	$\frac{\pi}{2}$	0	$q_1 + \frac{\pi}{2}$
3	0	$\frac{\pi}{2}$	0	$q_2 + \frac{\pi}{2}$
4	0	$\frac{\pi}{2}$	d_3	$q_3 + \frac{\pi}{2}$
5	0	$\frac{\pi}{2}$	0	q_4
6	0	0	d_5	q_5

The exoskeleton consists of three cuffs - the shoulder cuff, the upper arm cuff and the forearm cuff. Seven cables are routed through these cuffs to drive the exoskeleton. Four of the seven cables terminate on the upper arm cuff. These control the shoulder motion. The remaining cables are routed through the upper arm cuff and terminate on the forearm. These control the motion of the two DOFs in the elbow and the forearm. Since the cable attachment positions play a vital role in the workspace of the exoskeleton [11], they are made adjustable. On the shoulder cuff, both radial and angular positions of cable attachment points are adjustable. For upper arm and forearm cuffs only angular positions are adjustable. Two extension bars are attached to the upper arm cuff to route the cables from the upper arm cuff to the forearm cuff. These prevent potential cable collision with the elbow during motion.

B. Electronics and System Detail

A photograph of the exoskeleton prototype is shown in Fig. 2. The exoskeleton is mounted on a robotic arm for laboratory testing. The robotic arm has an encoder on each joint to measure the joint angle. Seven Kollmorgan Goldline XT AC motors are used to drive the exoskeleton. They are placed on an aluminum frame as shown in Fig. 3. The motors are powered by Kollmorgan ServoStar CD amplifiers in torque mode. Customized cable reels (Fig. 3) are designed to 1) prevent the cable from wrapping upon itself and avoid jerky motion. 2) allow estimation of cable lengths for calculating the joint angles of a human subject during motion. Nylon-coated pre-stretched steel cables are used that provide high durability and low axial vibration. A rubber piece is placed under the cable reel to hold the cable and prevent it from uncoiling from the reel. The motors are direct drive with rated continuous torque of 2.7Nm. The cable reel has a diameter of 2.85 inches. The maximum continuous cable tension is around 75N. Between each cable and its termination point on the cuff, a load cell(Transducer Techniques MLP-50) is connected. It measures the cable tension on the cuff and is later used in controlling the tension. The load cell signals are amplified by TMO-1 load cell conditioners. A National Instrument PXI data acquisition and real-time control system is used for interface electronics and control of the exoskeleton.

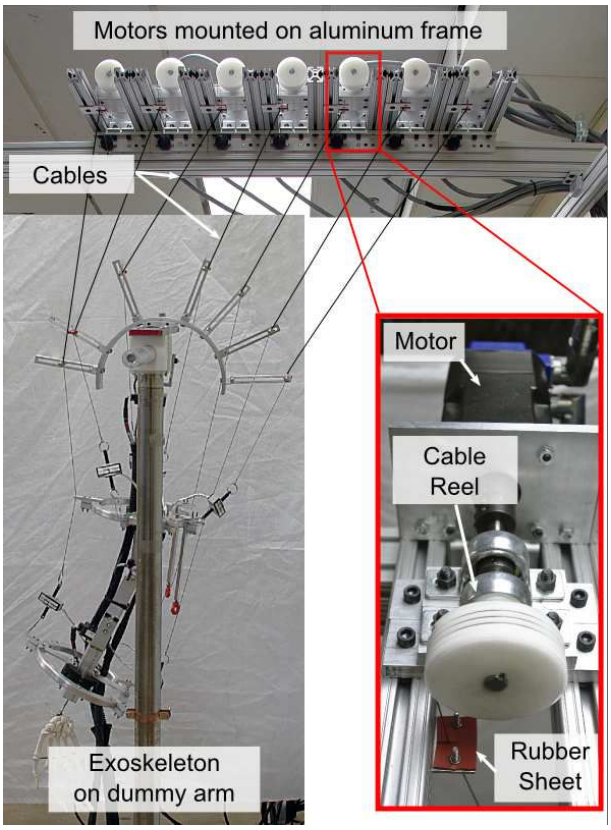

Fig. 3. A photograph of the arm exoskeleton mounted on a robotic arm and the customized cable reel.

C. Dynamic Model

The dynamic equations of motion for the 5-DOF upper arm exoskeleton are derived using Lagrangian method in

Maple. The generalized coordinates q_1, q_2, and q_3 represent shoulder flexion/extension, abduction/adduction and inward/outward medial rotation respectively. q_4 denotes the elbow flexion/extension. q_5 denotes the forearm pronation/supination. The equations of motion have the following form:

$$D(q)\ddot{q} + C(q,\dot{q})\dot{q} + g(q) = J(q)^T T(t) \tag{1}$$

where $q = (q_1, q_2, q_3, q_4, q_5)^T$ are the generalized coordinates, $D(q)$ is the 5×5 inertia matrix, $C(q,\dot{q})$ is the vector of coriolis and centripetal terms, $g(q)$ is the vector of gravity terms, $J(q)$ is a 7×5 Jacobian matrix relating cable tensions to joint moments, and $T(t)$ is the vector of cable tensions. The dynamic equations are fairly non-linear and complex, hence, only qualitative form of the dynamic equation is described in this paper.

D. Optimal cable tension planner

Due to the fact that cables can only pull but not push, the cable tensions must be kept positive for a cable-driven system to remain under control. Mathematically, the problem can be expressed as

$$AT = \tau, \tag{2}$$

where $A = J(q)^T$, Eq. (1), τ is computed from the left hand side of Eq. (1) and is function of $q(t)$, $\dot{q}(t)$, and $\ddot{q}(t)$. Eq. (2) is under-determined since the number of cables is greater than the number of DOFs. The solution of Eq. (2) can be written as

$$T = \bar{T} + N(A)\,m \tag{3}$$

where $\bar{T}$ is the minimum norm solution of Eq. (2) which is given by

$$\bar{T} = A^T\left(AA^T\right)^{-1}\tau \tag{4}$$

$N(A)$ is a 7×2 null space matrix of A and m is a 2×1 vector of arbitrary values, assuming A is full rank. On using constraints $T \in [T_{\min}, T_{\max}]$, the equivalent condition is

$$\begin{bmatrix} N(A) \\ -N(A) \end{bmatrix} m \geq \begin{bmatrix} T_{\min} - \bar{T} \\ -T_{\max} + \bar{T} \end{bmatrix} \tag{5}$$

An optimal set of cable tensions can be found using the following linear programming problem

$$\begin{aligned} &\min \sum_i \left(\bar{T} + N(A)\,m\right)_i \\ s.t.\quad &T_{\min} \leq \bar{T} + N(A)\,m \leq T_{\max}. \end{aligned} \tag{6}$$

This objective minimizes the sum of all cable tensions such that each cable tension falls within the tension limits $T_{\min}$ and $T_{\max}$. Optimization problem is formulated as a linear programming problem due to computational efficiency. One could also use other objective functions motivated by physical needs, e.g., maximize the safety indices for transmitted joint force and moment [13]. However, a nonlinear objective function would make the computation more intense.

TABLE II
TARGET JOINT RANGE OF MOTION FOR OPTIMIZATION

Joint		Range
Shoulder	q_1	$(-25°, 80°)$
	q_2	$(-140°, 25°)$
	q_3	$(-80°, 70°)$
Elbow	q_4	$(-150°, 0°)$
Forearm	q_5	$(-90°, 90°)$

III. WORKSPACE OPTIMIZATION FOR ADLS

The cable-driven upper arm exoskeleton is aimed at helping patients regain their ability to perform Activities of Daily Living. It would be desirable that the workspace allowed by the exoskeleton includes the workspace of the human hand to carry out most ADLs. However, this is difficult to accomplish due to unilateral actuation of cables.

The static workspace of the exoskeleton is a set of points in the Cartesian space where the arm can be held in equilibrium under gravity with cables in tension. Previous work has shown that a large static workspace increases the chance of satisfying cable tension constraints during dynamic motion [13]. Hence, the workspace must be optimized to ensure motion over a large workspace. In this work, the target range of motion of the joints is listed in Table II which covers 99% of ADLs [8]. We optimized the static workspace in this target space by proper selection of the cable attachment points on the three cuffs. For a given choice of cable attachment points, the target workspace of the exoskeleton was discretized. The static workspace was computed by counting the total number of feasible points at which the arm is able to stay in equilibrium under gravity ($\dot{q}, \ddot{q} = 0$). The cable attachment points were varied until an optimal solution was obtained. In the static workspace optimization, the following constraint on cable tensions were used: $T_{\min} = 1N$ and $T_{\max} = 75N$. The target workspace was discretized into 7776 configurations. The number of feasible configurations increased from $3136(40.3\%)$ before optimization to $6749(86.8\%)$ after optimization.

IV. CONTROLLER

A. Control Architecture

A two-level control architecture was implemented for the cable-driven upper arm exoskeleton; 1) a high-level force field controller [14] and 2) a low level cable tension controller. The force field controller planned the cable tensions to create a tunnel-like force field around the hand. The low level tension controller takes the cable tension commands from the force field controller and follows it to compensate for friction and other drive train losses. The control architecture is shown in Fig. 4

B. Cable Tension Controller

The goal of the low level cable tension controller is to make the cable tensions follow a reference command by adjusting the torque outputs of the motors. The controller is comprised of two parts: 1) Friction and reference feedforward and 2) Closed-loop PI control with in-line load cell.

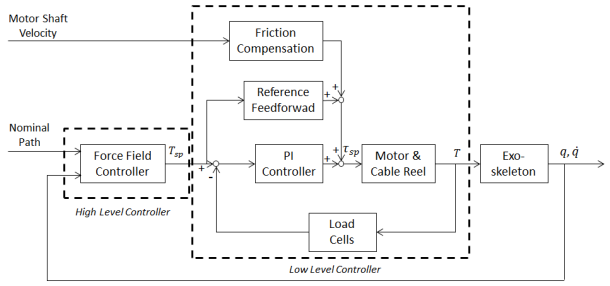

Fig. 4. Control system block diagram.

Since large AC motors are used, they introduce significant friction. The friction for each motor was estimated using the model described in Section IV-B.1. Given the reference cable tension, the required motor torque command were estimated using experimentally determined motor torque constants. These were fed-forward to the motor to produce the reference cable tensions. However, both the motor friction model and the motor torque constant have errors. Also, there are other unmodeled drive train losses, such as friction between cables and routing rings. These errors are compensated with the closed-loop PI controller. A load cell was connected along each cable close to its termination point to provide feedback for the controller. The PI controller can be implemented without friction and reference feed-forward, however having these in the loop allows faster response of the PI loop.

1) Motor Friction Compensation: To estimate motor friction, the following model was used.

$$f = \begin{cases} f_{sp} \cdot sign\left(v\right) + k_{vp} \cdot v & v \geq 0 \\ f_{sn} \cdot sign\left(v\right) + k_{vn} \cdot v & v < 0 \end{cases} \tag{7}$$

where f is the friction, f_{sp}, f_{sn} and k_{vp}, k_{vp} are parameters to be determined, and v is the motor shaft velocity. The relationship between f and v was measure by running a motor at different velocities and recording its motor currents. The corresponding friction was determined using torque constant of the motor. The parameters in the model were chosen to fit the data. A typical plot of f and v is shown in Fig. 5. This friction model gives only an estimate of the friction. This model was used with the PI controller.

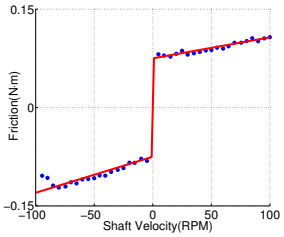

Fig. 5. Motor shaft friction curve as a function of shaft velocity. In this case, the fitted model is: $f = 0.075 + 0.0032 \cdot v$ for $v \geq 0$ and $f = -0.075 + 0.0055 \cdot v$ for $v \leq 0$.

C. Force Field Controller

During training, a subject will be asked to follow a pre-planned nominal path using the hand, i.e., move a ball from one point to another following a prescribed path. Due to the existence of infeasible configurations, not all paths are admissible. A feasible path can be generated by varying the shape of the path through optimization [13]. The force field controller creates a tunnel-like force field around the nominal path to provide assistance to a subject [14]. Fig. 1 shows the typical shape of the three dimensional force tunnel. If the hand of the subject lies in the tunnel, the force field applies a tangential force F_t on the hand to keep the hand moving along the nominal path. If the hand moves out of the tunnel, a normal force F_n is applied to help the subject move back into the tunnel. A damping force F_d is always applied to reduce oscillations. The total force applied to the hand is given by

$$F = F_t + F_n + F_d. \tag{8}$$

Let P be the current position of the hand in the inertial frame and N be the closest point to P on the nominal path (See Fig.1). The direction of the normal force is defined by $\hat{n}$ which is the normal vector from P to N. The direction of the tangential force is defined by the normal vector $\hat{t}$ tangential to the nominal path at N. The three force components F_t, F_n, and F_d are defined as following

$$F_t = \begin{cases} K_t \left(1 - \frac{d}{D_t}\right) \vec{t}, & d < D_t \\ 0, & d \geq D_t \end{cases}, \tag{9}$$

$$F_n = K_n \frac{1}{1 + e^{-Ns(d - D_n)}}, \tag{10}$$

$$F_d = -K_d \cdot v, \tag{11}$$

where K_t, K_n, K_d are gains for corresponding force components, d is the distance from P to N, D_t is the radius of the tangential force tunnel. D_n is the radius of the normal force tunnel. Ns determines the slope of the normal force tunnel, and v is the velocity of the hand.

The required joint torques τ_w to generate the force field is given by

$$\tau_w = J_e^T\left(q\right) F \tag{12}$$

where J_e^T is the Jacobian matrix of the hand. The required cable tensions are found by solving

$$J^T\left(q\right) T = \tau_w + g\left(q\right), \tag{13}$$

using the algorithm proposed in Section II-D. The gravity vector $g(q)$ is added to compensate for the gravity of the exoskeleton.

D. Simulation

In the simulation, a straight line nominal path of the hand was created to simulate an Activity of Daily Living. To simulate the abnormal hand movement pattern, a hand motion trajectory was prescribed to follow a reference path outside the tunnel. A PD controller controlled the arm to follow the trajectory. Then the force field controller was implemented to assist the arm motion. The simulation results

TABLE III

SUMMARY: 5 SESSIONS FOR EACH TASK

Session	Force Field Gain	Gravity compensation
1	$K_n = 0.5N$	Yes
2	$K_n = 2.0N$	Yes
3	$K_n = 3.5N$	Yes
4	$K_n = 0N$	Yes
5	$K_n = 0N$	No

are shown in Fig. 6. Parameters used for the force field controller are: $K_t = 0.001$, $K_d = 0.1$, $Kn = 50$, $D_n = 0.01m$. The force field controller was able to keep the hand closer to the nominal path.

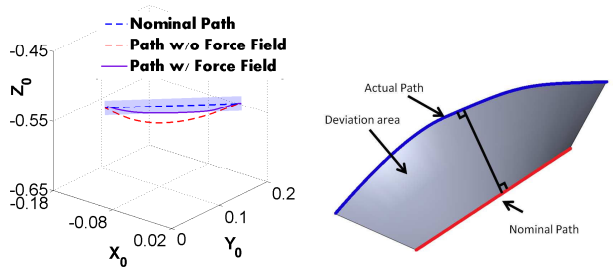

Fig. 6. Left: Simulation results of the force field controller. Right: The deviation area is formed by normal lines between the actual path and nominal path.

E. Experiment

Five healthy subjects evaluated the exoskeleton. Subjects operated the exoskeleton with two external cables connected to the top of the exoskeleton (Fig.7). For each task, two rubber bars are clamped on a retort stand at different locations. The subjects were asked to move the end-effector to from one rubber bar to the other. The straight line connecting the two tips was used as the nominal path for the force field controller. Each subject carried out 2 different tasks (Fig. 7). Each task included 5 sessions with different controller parameters listed in Table III. The other force field controller parameters are the same for all trials: $D_n = 0.007$, $N_s = 700$, $K_d = 0$, $K_t = 0$. The gains for the cable tension controllers were $K_p = 10$ and $K_i = 0.01$. The first three sessions featured weak to strong normal forces. In the fourth session, the force field was turned off leaving only gravity balancing. The last session had no force assistance. In each session, the subject performed the same task 6 times. Before the evaluation, the subjects were instructed with the following guidelines:

- Move the end-effector from one rubber bar to the other
- Move the hand at moderate speed (around $15cm/s$).
- Perform the task twice before each session to get familiar with the setup.

The performance of each trial was measured by computing the deviation area of the actual path of the end-effector from the nominal path[18]. This is illustrated in Fig. 6. The deviation area was computed for each session and then averaged over trials. The experimental results for task 1 of Subject 2 are shown in Fig. 8.

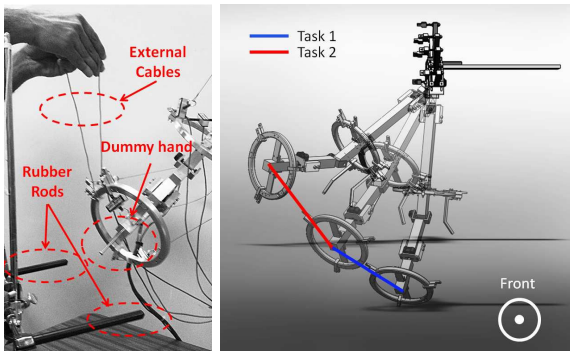

Fig. 7. Left: A subject operating the exoskeleton with two cables. Right: Two tasks used in the experiment. Task 1: Path length = 0.24m. Task 2: Path length = 0.26m

TABLE IV

PAIRED T-TEST RESULTS FOR TWO TASKS

	$0.5N$ vs. G	NA vs. G	2N vs. 3.5N	3.5N vs. NA
Task 1	-	-32.96% $p = 0.0411$	-	-30.91% $p = 0.0516$
Task 2	-	-	-	-22.85% $p = 0.0442$

Note: $0.5N$: $K_n = 0.5N$, Session 1. $2N$: $K_n = 2.0N$, Session 2. $3.5N$: $K_n = 3.5N$, Session 3. G: Gravity balancing only, Session 4. NA: No Assist, Session 5.

For each task, the results were statistically analyzed using paired t-test to compare the results between sessions. The threshold for p value was selected to be 6% for all tests.

Results of the paired t-test are shown in Table IV. If the t-test result is shown with a (-), it means that the mean of the two sets of data are similar. Otherwise, the percentage decrease data isshown in the table with the p value. The following observations were obtained from the statistical tests:

- Gravity only session and $K_n = 0.5N$ session had similar performance. It was possibly due to the fact that the normal force is weak.
- The sessions $K_n = 2.0N$ and $K_n = 3.5N$ had no significant difference in their means resulting in similar performance.
- For sessions $K_n = 3.5N$, the mean deviation area among subjects reduced by 22.85%-30.91% when compared with the 'No Assistance' sessions. This indicated that with the force field controller, the subjects were able to move the arm closer to the nominal path.

V. CONCLUSION AND FUTURE WORK

A 5-DOF cable-driven upper arm exoskeleton targeting patient training was designed and built. The system is capable of controlling cable tensions with the aid of in-line load cells. Its static workspace was optimized to achieve large a range of motion for Activities of Daily Living. Force field control architecture was proposed for this system. Simulation has shown that the force field controller performs well in assisting the hand motion along a nominal path. Experiments were carried out by health subjects to validate the design.

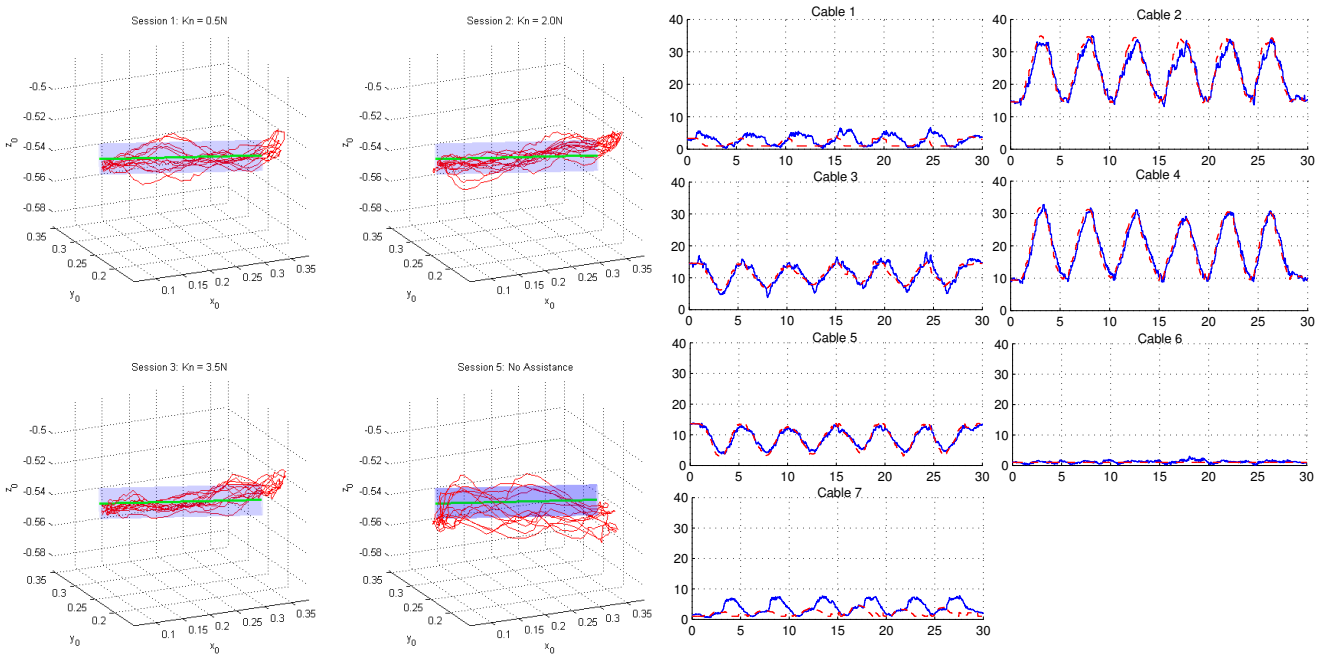

Fig. 8. Left: Paths of the dummy hand (red) against nominal path (green) for 5 sessions. Right: Actual cable tensions (blue) against cable tension references(red) during session 1.

Results show that the force field controller is able to increase the performance of healthy subjects in the tasks presented.

Currently, additional experiments are planned to evaluate the performance of the controller when tangential force and damping force are employed. The interface between the exoskeleton and human is under development. Experiments with human subjects wearing the exoskeleton is planned in the near future.

Acknowledgement: The authors would like to thank Steve Beard from Student Machine Shop for his kind support in manufacturing the exoskeleton. The support of this work from an NIH INBRE grant to University of Delaware is gratefully acknowledged.

REFERENCES

[1] C. Butefisch, H. Hummelsheim, P. Denzler, and K.-H. Mauritz, "Repetitive training of isolated movements improves the outcome of motor rehabilitation of the centrally paretic hand," *Journal of the Neurological Sciences*, vol. 130, no. 1, 1995.

[2] M. L. Aisen and H. I. Krebs, "The effect of robot-assisted therapy and rehabilitative training on motor recovery following stroke," *Stroke*, vol. 28, 1997.

[3] G. Kwakkel, R. C. Wagenaar, T. W. Koelman, G. J. Lankhorst, and J. C. Koetsier, "Effects of intensity of rehabilitation after stroke," *Archives of Neurology*, vol. 54, no. 4, 1997.

[4] D. Reinkensmeyer, S. Lehman, and P. Lum, "A bimanual therapy robot: controller design and prototype experiments," *IEEE International Conference on Rehabilitation Robotics*, pp. 938 –939, 1993.

[5] T. Nef and R. Riener, "Armin - design of a novel arm rehabilitation robot," *IEEE International Conference on Rehabilitation Robotics*, pp. 57–60, 2005.

[6] C. Carignan, M. Liszka, and S. Roderick, "Design of an arm exoskeleton with scapula motion for shoulder rehabilitation," *International Conference on Advanced Robotics*, pp. 524–531, 2005.

[7] A. Gupta and M. K. O'Malley, "Design of a haptic arm exoskeleton for training and rehabilitation," *IEEE/ASME Transactions on Mechatronics*, vol. 11, pp. 280–289, 2005.

[8] J. C. Perry, J. Rosen, and S. Burns, "Upper-limb powered exoskeleton design," *IEEE/ASME Transactions on Mechatronics*, vol. 12, pp. 408–417, 2007.

[9] S. Ball, I. Brown, and S. Scott, "Medarm: a rehabilitation robot with 5dof at the shoulder complex," *IEEE/ASME international conference on Advanced intelligent mechatronics*, pp. 1–6, 2007.

[10] G. Yang, H. L. Ho, W. Chen, W. Lin, S. H. Yeo, and M. Kurbanhusen, "A haptic device wearable on a human arm," *IEEE Conference on Robotics, Automation and Mechatronics* Dec. 2004.

[11] S. Agrawal, V. Dubey, J. Gangloff, E. Brackbill, Y. Mao, and V. Sangwan, "Design and optimization of a cable driven upper arm exoskeleton," *Journal of Medical Device*, vol. 3, p. 031004, 2009.

[12] E. Brackbill, Y. Mao, S. Agrawal, M. Annapragada, and V. Dubey, "Dynamics and control of a 4-dof wearable cable-driven upper arm exoskeleton," *IEEE International Conference on Robotics and Automation*, pp. 2300–2305, 2009.

[13] Y. Mao and S. Agrawal, "Wearable cable-driven upper arm exoskeleton - motion with transmitted joint force and moment minimization," *IEEE International Conference on Robotics and Automation*, pp. 4334–4339, 2010.

[14] S. K. Banala, S. H. Kim, S. K. Agrawal, and J. P. Scholz, "Robot assisted gait training with active leg exoskeleton (alex)," *IEEE Transactions on Neural Systems and Rehabilitation Engineering*, vol. 17, no. 1, 2008.

[15] S. Oh and S. Agrawal, "Cable suspended planar robots with redundant cables: controllers with positive tensions," *IEEE Transactions on Robotics*, vol. 21, no. 3, pp. 457 – 465, Jun. 2005.

[16] S. Oh and S. Agrawal, "Generation of feasible set points and control of a cable robot," *IEEE Transactions on Robotics*, vol. 22, no. 3, pp. 551 – 558, Jun. 2006.

[17] S. Oh and S. Agrawal, "The feasible workspace analysis of a set point control for a cable-suspended robot with input constraints and disturbances," *IEEE Transactions on Control Systems Technology*, vol. 14, no. 4, pp. 735 – 742, Jul. 2006.

[18] S. Agrawal,X. Chen,J. Galloway, "Training Special Needs Infants to Drive Mobile Robots Using Force-Feedback Joystick," *IEEE International Conference on Robotics and Automation*, pp. 4797–4802, 2010.